Performance Analysis of FBMC and CP-OFDM in the Presence of Phase Noise

Kilian Roth*†, Leonardo Gomes Baltar*, Michael Faerber*, Josef A. Nossek†‡

* Next Generation and Standards, Intel Deutschland GmbH, Neubiberg, Germany
Email: {kilian.roth, leo.baltar, michael.faerber}@intel.com
† Department of Electrical and Computer Engineering, Technical University Munich, Munich, Germany
Email: {kilian.roth, josef.a.nossek}@tum.de
‡ Department of Teleinformatics Engineering, Federal University of Ceara, Fortaleza, Brazil

***Abstract*—Multi-Carrier (MC) modulation schemes like Orthogonal Frequency Division Multiplexing (OFDM) are highly sensitive to Phase Noise (PN). In the case of air interfaces operating in higher frequencies, e.g. the range between 6 and 100 GHz frequently called millimeter wave (mmWave), the PN generated by the local oscillators is even more accentuated. Alternative MC systems are being considered for future mmWave wireless communications. In this contribution, we analytically derive expressions for an upper bound for the interference power generated by the PN in OFDM, DFT-Spread-OFDM and Filter Bank Multi-Carrier (FBMC). Then, we evaluate the performance degradation due to that imperfection in terms of coded and uncoded BER.**

I. Introduction

For the next generation mobile broadband standard (aka. 5G) higher carrier frequencies are being considered [1]. These frequencies are in the range of 6 to 100 GHz. In general, this frequency range is referred to as millimeter wave, even though it contains the lower centimeter wave range. The major advantage is the large available bandwidths in this spectrum range.

LTE, LTE-Advanced (aka. 4G) and WiFi systems operating below 6 GHz employ CP-OFDM based MC modulation schemes. Other MC schemes like FBMC are currently being considered for future wireless standards. In general, MC modulation schemes have the advantage of improved performance in frequency selective fading environment, especially if combined with channel coding. In a multi-user environment, frequency dependent scheduling and resource allocation help leveraging the best parts of the spectrum for every user. This features come at the price of an increased sensitivity to synchronization errors and nonlinearities of the Radio Frequency (RF) front-end. For example, MC systems are more sensitive to RF impairments like PN, because it destroys the orthogonality between subcarriers and introduces Inter-Carrier Interference (ICI).

The PN encountered in a Voltage Controlled Oscilator (VCO) increases with the oscillating frequency [2]. Additional quality of the VCO increases the power consumption. Today even low-cost low-power CMOS VCOs for mmWave consume a considerable amount of power [3]. Therefore, it will not be possible to design mmWave VCOs with a similar power consumption and PN property as VCOs used in LTE devices today.

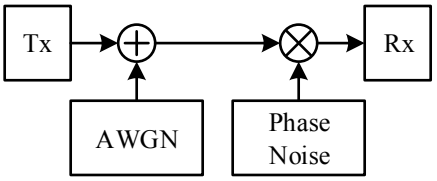

Fig. 1. Phase noise equivalent baseband model.

In this paper, we analyze the sensitivity to PN of conventional OFDM, DFT-S-OFDM and FBMC by considering PN characteristics of existing VCOs for mmWave at 60 GHz. We first derive analytical formulas for the power of the ICI due to PN and then numerically evaluate the performance of the MC systems.

II. Inter-Carrier Interference due to Phase Noise

Fig. 1 shows the equivalent baseband model of a SISO system with AWGN channel and phase noise at the receiver. The phase noise is a random phase rotation applied in the time domain. From Fourier analysis, it is known that a phase shift in time domain represents a frequency shift in the frequency domain. Therefore, it can be shown that phase noise generates many frequency shifted replicas of the original signal spectrum that are then added to the original signal. This generates ICI in a MC system, especially if it has a poor frequency localization, like conventional OFDM.

Based on this observation, we derive a lower bound on the ICI power and, therefore, an upper bound on the achievable SINR without PN compensation, which represents a best case scenario. First, the contribution to the desired signal of each frequency offset is calculated. Afterwards, this contribution is integrated over the Power Spectral Density (PSD) of the PN. For this calculation, we assume that all contributions add up coherently, therefore, the derived formula is a lower bound of the interference power. The PN of an oscillator is measured in dBc, where the reference is the desired carrier frequency. To predict the performance of an OFDM, DFT-s-OFDM and

978–1–5386–3873–6/17/$31.00 ©

FBMC system in the presence of phase noise, we calculate the ICI power from the measured phase noise power spectral density.

In an MC system the received symbol $R_{k,\ell}$ after the demodulation on subcarrier k and on symbol ℓ can be defined as

$$R_{k,\ell} = e^{j\phi_\ell(\epsilon)}\alpha(\epsilon)H_{k,\ell}X_{k,\ell} + I_{k,\ell}(\epsilon) + W_{k,\ell}. \quad (1)$$

Here $X_{k,\ell}$, $H_{k,\ell}$, $W_{k,\ell}$ and $I_{k,\ell}(\epsilon)$ represent the transmitted signal, the channel, the AWGN and the interference cause by the frequency offset. The coefficient $\alpha(\epsilon)$ represents the attenuation of the signal and the frequency offset ϵ is normalized by the subcarrier spacing.

For the following derivations, we assume that the effects of the channel $H_{k,\ell} = 1$ are perfectly compensated by channel estimation and ZF-equalization for all k and ℓ, i.e. for mildly frequency selective channels. This will also include the common phase error $e^{j\phi_\ell(\epsilon)}$. We can then reduce (1) to

$$R_{k,\ell} = \alpha(\epsilon)X_{k,\ell} + I_{k,\ell}(\epsilon) + W_{k,\ell}. \quad (2)$$

The PSD of an FBMC transmit signal with N subcarriers, subcarrier spacing Δf and overlapping factor M is defined for each subcarrier as

$$x_{\text{Tx}}(f) = \sum_{m=-(M-1)}^{M-1} g_m \frac{\sin\left(\pi\left(\frac{fM}{\Delta f} - m\right)\right)}{\sin\left(\pi\left(\frac{fM}{\Delta f} - m\right)/(MN)\right)MN}, \quad (3)$$

where the g_ms are the filter coefficients in the frequency domain and f the frequency variable. Here, we are only interested in the shape of the PSD of the transmitted signal, therefore, this formula does not contain the symbols transmitted in each subcarriers, which are assumed to be uni-modular constants.

The receive signal is filtered by the discrete time receive filter $G_{\text{Rx}}(f)$ defined as

$$G_{\text{Rx}}(f) = \sum_{m=-(M-1)}^{M-1} g_m \delta\left(f - \frac{m\Delta f}{M}\right), \quad (4)$$

where $\delta(f)$ is a Dirac impulse. The signal attenuation $\alpha(\epsilon)$ due to a frequency offset ϵ can be calculated as

$$\alpha(\epsilon) = \int_{-\infty}^{\infty} x_{\text{Tx}}(f + \epsilon\Delta f)G_{\text{Rx}}(f)df. \quad (5)$$

If we plug-in the definition of $G_{\text{Rx}}(f)$ from (4) into (5), the integral is reduced to the sum

$$\alpha(\epsilon) = \sum_{m_{\text{Rx}}=-(M-1)}^{M-1} g_{m_{\text{Rx}}} x_{\text{Tx}}\left(\frac{m_{\text{Rx}}\Delta f}{M} + \epsilon\Delta f\right). \quad (6)$$

By plugging (3) into (6) we get (7). For the special case of a conventional OFDM system, M is equal to one and (7) is reduced to

$$\alpha(\epsilon) = \frac{\sin(\pi\epsilon)}{\sin(\pi\epsilon/N))\,N}, \quad (8)$$

which is the same result presented in [4]. It is important to keep in mind that, without frequency offset there is no attenuation of the signal, i.e. $\alpha(0) = 1$.

In general, the phase noise is described by its PSD $S(\epsilon)$. Two examples showing typical normalized PN PSDs are shown in Fig. 2. By integrating over the contributions at each frequency offset, we can calculate the upper bound of the signal attenuation A after demodulation and in the presence of phase noise. A is then given by

$$A \leq P_{fc} + 2\int_0^{\epsilon_{\text{max}}} \alpha^2(\epsilon)S(\epsilon)d\epsilon, \quad (9)$$

where P_{fc} is the power at the carrier frequency. This calculation assumes that the contributions to the desired signal from each frequency offset add up coherently. Therefore, the presented formula is an upper bound of the signal power and, the more components contribute to it, the looser this bound will get. Since the phase noise is assumed to be symmetric, it is sufficient to integrate from 0 to ϵ_{max} and multiply the result by two. The value of $S(\epsilon)$ at $\epsilon = 0$ is zero, because this is the desired signal and, consequently, not part of the PSD of the PN. As the PN is a random phase rotation of the signal, it does not change the power of the signal. Because the PSD of the phase noise is usually measured in relative power levels (dBc), we need to convert them to absolute power levels. First, we need to calculate the integrated PN power relative to the carrier frequency power

$$P_r = 2\int_0^{\epsilon_{\text{max}}} S_r(\epsilon)df. \quad (10)$$

The total power should stay constant and, as a consequence, the sum of the power at the carrier frequency P_{fc} plus the power of the PN P must be equal to one, i.e.

$$P_{fc} + P = 1. \quad (11)$$

The term P can be replaced by $P_r P_{fc}$. Then (11) can be reformulated to

$$P_{fc} = \frac{1}{1 + P_r}. \quad (12)$$

With this result we can calculate the PSD $S(\epsilon)$ out of the measured relative PSD $S_r(\epsilon)$. Now, we have obtained all necessary components of (9), which changes to

$$A \leq P_{fc}\left(1 + 2\int_0^{\epsilon_{\text{max}}} \alpha^2(\epsilon)S_r(\epsilon)d\epsilon\right) \quad (13)$$

after considering the relative PSD of the PN.

If we assume that the transmit signal power is σ_s^2, the signal and noise power after demodulation are bounded by

$$P_S \leq A\sigma_s^2 \quad \text{and} \quad P_I \geq (1 - A)\,\sigma_s^2. \quad (14)$$

The SIR represents the maximum system SINR in the high SNR regime, if the system is limited by the PN, i.e.

$$\text{SIR} \leq \frac{P_S}{P_I}. \quad (15)$$

$$\alpha(\epsilon) = \sum_{m_{\mathrm{Rx}}=-(M-1)}^{M-1} g_{m_{\mathrm{Rx}}} \sum_{m_{\mathrm{Tx}}=-(M-1)}^{M-1} g_{m_{\mathrm{Tx}}} \frac{\sin\left(\pi\left(m_{\mathrm{Rx}} - m_{\mathrm{Tx}} + \epsilon M\right)\right)}{\sin\left(\pi\left(m_{\mathrm{Rx}} - m_{\mathrm{Tx}} + \epsilon M\right)/\left(MN\right)\right) MN}. \tag{7}$$

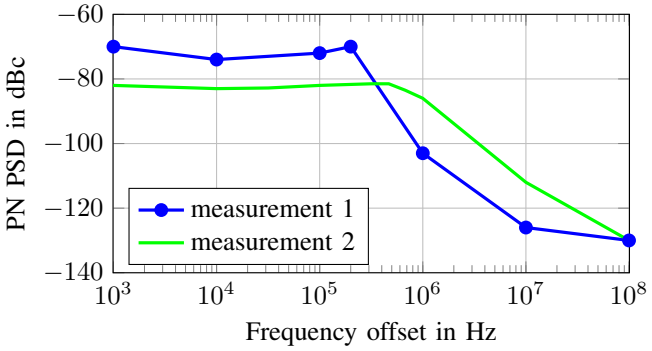

Fig. 2. Phase noise PSD measurements.

Now, we compare the results of the theoretically calculated interference power to the results of a Monte Carlo simulation, where the PN is modeled according to the equivalent baseband model in Fig. 1. The phase noise is generated by taking Gaussian noise and then shaping it in the frequency domain according to the PSD of the phase noise. Afterwards, we convert it to the time domain. This generation process has the disadvantage that, if the linear spacing of the frequency domain samples become too large, it will not be possible to completely cover the shape of the PSD. This means that the model becomes less and less accurate the higher the subcarrier spacing is.

The PN PSDs are taken from the examples of oscillators at 60 GHz in Fig. 2. The filter described in [5] with M equal to 2 is used in the FBMC system. In the simulations, the inter-carrier interference is calculated in a system without AWGN. In this high SNR regime, the system performance is limited by the interference power, as a consequence, the SIR is shown and compared to the theoretically calculated SIR. The results are shown in Figs. 3 and 4 for the same PN PSDs with different carrier spacing Δf. We can see that the PN power close to the carrier frequency is higher for measurement 1, but it starts to decrease rapidly after 200 kHz. In contrast, the PN power of measurement 2 remains almost constant until 1 MHz. This is also reflected in the simulated and calculated phase noise power in Figs. 3 and 4 for different subcarrier spacings. We can clearly see that for measurement 1, the SIR is much smaller if the carrier spacing is small. But as soon as the subcarrier spacing reaches 0.5 MHz, the performance is better compared to the phase noise in measurement 2.

In Figs. 3 and 4, for a certain range of subcarrier-spacing, the bound is tight to the simulated results. Another reason for the increasing gap between the simulation and the analytical upper bound is the model of the colored noise. The higher the sampling frequency and, therefore, the subcarrier spacing Δf, the more problematic it is to model the colored noise by a filtered AWGN noise. Overall, we can see that FBMC offers a similar robustness towards PN compared to CP-OFDM for the setup evaluated.

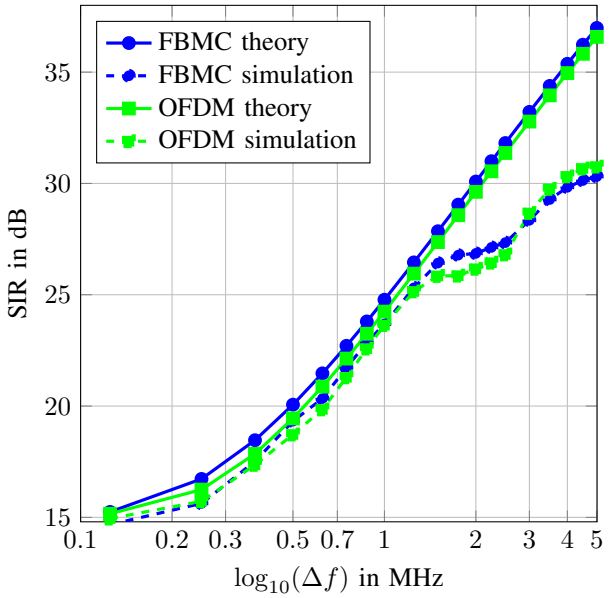

Fig. 3. SIR phase noise with different subcarrier spacings, PN PSD 1

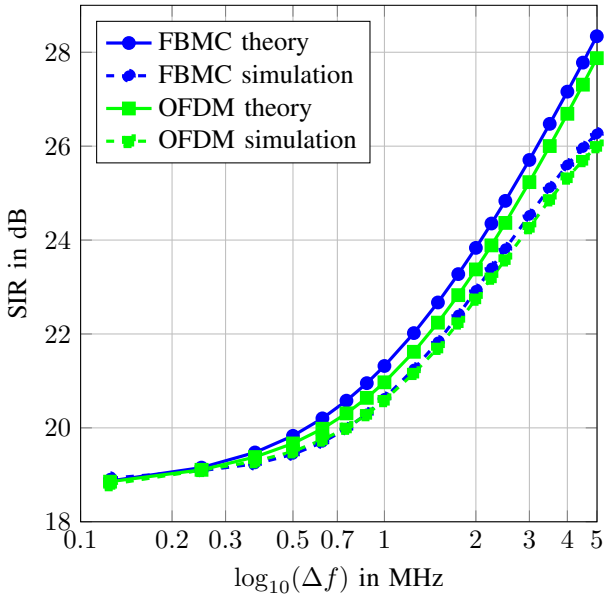

Fig. 4. SIR phase noise with different subcarrier spacings, PN PSD 2

III. Coded and uncoded BER Results

In a MC system with PN, the interference does not necessarily follow a Gaussian distribution. For OFDM, the authors of [6] showed that the probability density function (PDF) of the ICI in an OFDM system has a much stronger tail than in the Gaussian distribution. Due to the fact that in FBMC the symbols are spread over a longer period of time, there are more independent symbols contributing to the ICI. This means that according to the Central Limit Theorem (CLT) [7], the PDF of the ICI converges closer to a Gaussian distribution, therefore, the tail of the PDF is similar to the one of a Gaussian

distribution. A detailed investigation of this matter is left for a future contribution.

The symbols on adjacent subcarriers are assumed to be uncorrelated, so in the case of OFDM and FBMC the ICI is also uncorrelated. On the other hand, in the case of DFT-s-OFDM, the signals on adjacent subcarriers are correlated and therefore the interference is correlated. The additional DFT despreading operation provokes a random phase shift of the signal and additional noise. This phase shift depends on the actual transmitted symbol and the effect of PN on DFT-s-OFDM is, consequently, similar to the effect on a single carrier modulation with additional interference.

The difference between the modulation schemes can be seen in Fig. 5, where the uncoded BER performance of the three different systems with and without PN are shown. We have used in the simulations a 16-QAM constellation and a subcarrier spacing of $\Delta f = 0.75$ MHz. We can conclude that the performance of FBMC, OFDM and DFT-s-OFDM over a AWGN channel is the same and, therefore, from now on only the case of OFDM without PN is shown as a reference. We can clearly see that at the point where the PN becomes the dominant source of error, the BER performance of FBMC further improves, while the performance of OFDM and DFT-s-OFDM starts to saturate. In comparison with OFDM, the DFT-s-OFDM performance is worse in terms of uncoded BER. This is because the phase rotation brings the symbol closer to the decision border than a Gaussian noise would do.

The differences between FBMC, OFDM and DFT-s-OFDM can be more clearly seen in the coded BER evaluation. We have used here the turbo code with rate matching defined in the LTE standard [8]. Moreover, we have employed subcarrier spacing of Δf =0.75 MHz and 1.5 MHz with the PN measurement 2 shown in Fig. 2.

Figs. 6 and 7 show the coded BER performance for 64-QAM with various code rates. The coding rates $\{0.36, 0.43, 0.50, 0.59, 0.66, 0.74\}$ were used. We can see that, as we increase the code rate, the additional interference introduced by the PN has a larger impact on the coded BER performance. As the code rate gets higher, the performance gain of FBMC becomes more and more visible. In fact, for high coding rates in the 64-QAM case, the coded BER performances of FBMC shows no error floor above 10^{-4}. In the case of OFDM and DFT-s-OFDM, this error floor is relatively high. There are two reasons why FBMC has a substantially better performance than OFDM for high code rates. First, as shown in Fig. 5, at the SNR range where the uncoded BER performance is dominated by the PN, FBMC has a lower BER. The second reason is that, if a bit error occurs, FBMC has a much lower probability of surpassing the decision by a very large amount, which OFDM has due to its thicker tail in the ICI CDF shown in Fig. 8.

IV. Conclusion

We have shown that phase noise has a severe impact on the performance of multicarrier systems. Especially in the high SNR regime, where the performance will be limited by the ICI.

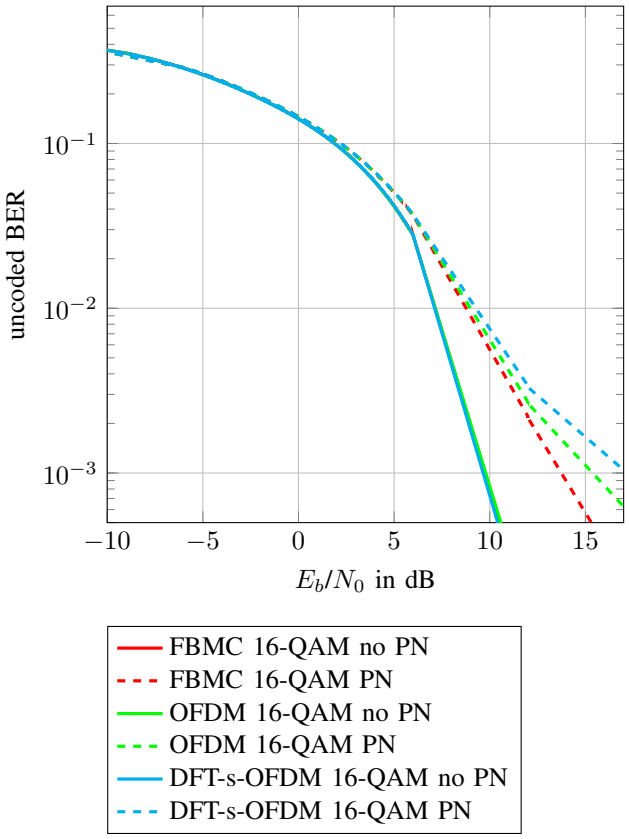

Fig. 5. Uncoded BER, $\Delta f = 0.75$ MHz and 16-QAM.

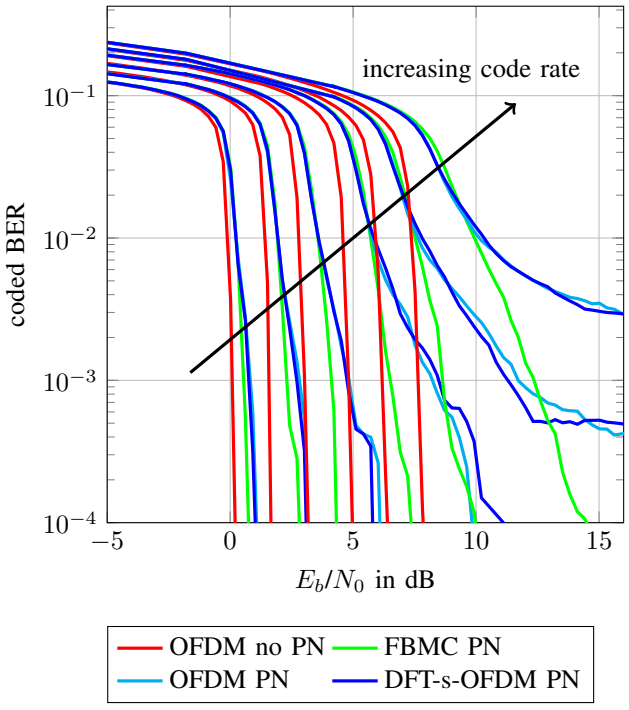

Fig. 6. Coded BER, Δf 0.75 MHz, 64-QAM and different coding rate.

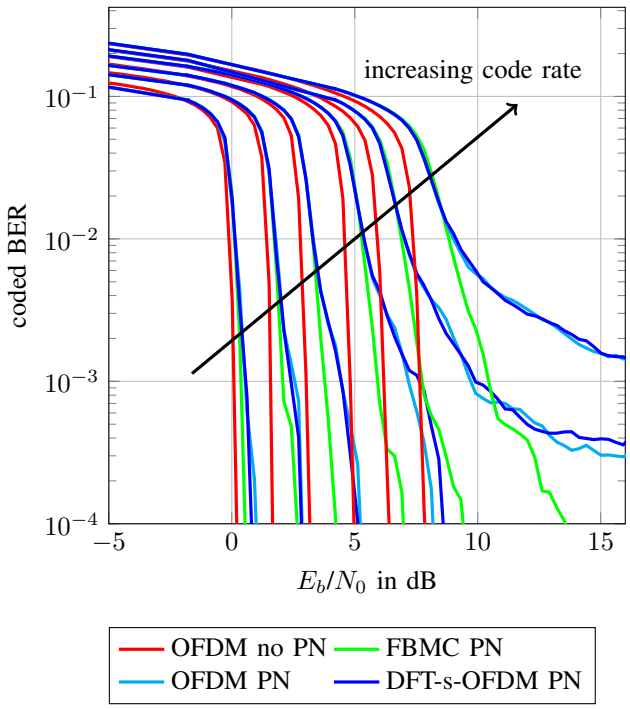

Fig. 7. Coded BER, Δf 1.5 MHz, 64-QAM and different coding rate.

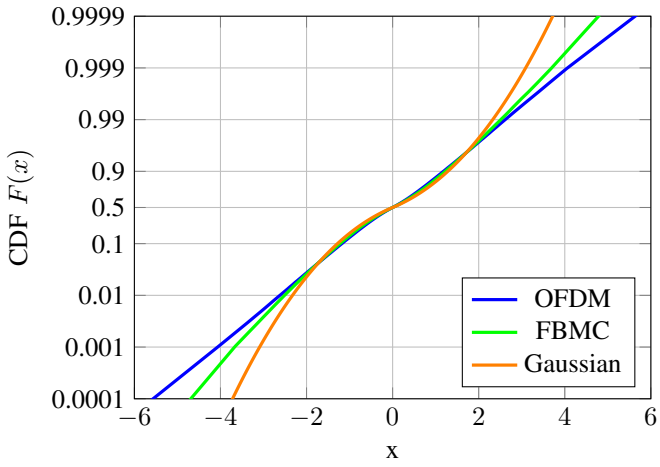

Fig. 8. ECDF of OFDM and FBMC ICI compared to a Gaussian random variable.

We derived a method to analytically calculate an upper bound of the ICI power and compared it with Monte Carlo based simulations. In the case of smaller subcarrier spacing, the results agree quite well. Therefore, this calculation method can be used to evaluate the performance impact of the subcarrier spacing in an MC system.

Since choosing a subcarrier spacing has a strong impact on the behavior of the system, in many ways this enables a fast theoretical evaluation of the performance depending on the PN. Finally, we have showed that the performance of FBMC is only significantly superior to OFDM and DFT-s-OFDM, if the coding rate is relatively high. It is worth noting that, we have not considered here the loss of spectral efficiency resulting from a CP that is necessary in OFDM systems operating in multipath fading channels.

The constraints on the subcarrier spacing of OFDM and FBMC are quite different. For an OFDM system, it is essential to make the subcarrier spacing as small as possible to limit the overhead of the CP. But this makes OFDM more sensitive to PN and synchronization errors. Therefore, to design an OFDM system, only a careful evaluation of this trade-off leads to a good performance in the desired scenarios. In contrast, an FBMC system does not need a CP, thus only the scheduling granularity and the desired length of the equalizer for each subcarrier puts an upper limit to the subcarrier spacing. Overall, that means an FBMC system should have a larger subcarrier spacing than an OFDM system for the same application. This leads to more robustness towards PN and synchronization errors.

Acknowledgment

This work was supported by the European Commission in the framework of the H2020-ICT-2014-2 projects Flex5Gware (Grant agreement no. 671563) and mmMAGIC (Grant agreement no. 671650).

References

[1] F. Boccardi et al., "Five disruptive technology directions for 5G," *IEEE Commun. Mag.*, vol. 52, no. 2, pp. 74–80, Feb. 2014.

[2] A. M. Niknejad et al., "A circuit designer's guide to 5G mm-wave," in *Custom Integrated Circuits Conf. (CICC) 2015*, San Jose, CA, California, Sept. 2015, pp. 1–8.

[3] Tianzuo Xi et al., "Low-phase-noise 54GHz quadrature VCO and 76GHz/90GHz VCOs in 65nm CMOS process," in *Radio Frequency Integrated Circuits Symp. (RFIC) 2014*, Tampa, FL, USA, June 2014, pp. 257–260.

[4] M. Morelli et al., "Synchronization techniques for orthogonal frequency division multiple access (OFDMA): a tutorial review," *Proc. IEEE*, vol. 95, no. 7, pp. 1394–1427, July 2007.

[5] M. Bellanger, "FBMC physical layer : a primer," June 2010. [Online]. Available: http://www.ict-phydyas.org

[6] D. Petrovic, W. Rave and G. Fettweis, "Properties of the intercarrier interference due to phase noise in OFDM," in *Int. Conf. on Communications (ICC) 2005*, vol. 4, Seoul, Korea, May 2005, pp. 2605–2610 Vol. 4.

[7] W. Feller, "The fundamental limit theorems in probability," *Bull. Amer. Math. Soc.*, vol. 51, pp. 800–832, 1945.

[8] *Evolved universal terrestrial radio access (E-UTRA); multiplexing and channel coding*, 3rd Generation Partnership Project (3GPP) Std. 36.212, 2016. [Online]. Available: http://www.3gpp.org/ftp/Specs/html-info/36212.htm